Relationship between Structure and CO Oxidation Activity of Ceria-Supported Gold Catalysts

Anna Maria Venezia,*,† Giuseppe Pantaleo,‡ Alessandro Longo,† Gabriella Di Carlo,‡ Maria Pia Casaletto,† F. Leonarda Liotta,† and Giulio Deganello†,‡

Istituto per lo Studio dei Materiali Nanostrutturati, CNR, Via Ugo La Malfa 155, 90146 Palermo, Italy, and Dipart. Chimica Inorganica e Analitica, " S. Cannizzaro", Università di Palermo, V.le delle Scienze, Parco D'Orleans 90128 Palermo, Italy

Received: September 9, 2004; In Final Form: December 2, 2004

Gold catalysts supported on cerium oxide were prepared by solvated metal atom dispersion (SMAD), by deposition-precipitation (DP), and by coprecipitation (CP) methods and were characterized by X-ray diffraction (XRD), temperature programmed reduction (TPR), and X-ray photoelectron spectroscopy (XPS). The catalytic activity was tested in the CO oxidation reaction. The structural and surface analyses evidenced the presence of a modified ceria phase in the case of the DP sample and the presence of pure ceria and gold metal crystallites in the case of the SMAD and CP samples. The DP sample, after a mild treatment in air at 393 K, exhibited only ionic gold, and it was very active below 273 K. By comparing the activities of the different catalysts, it is suggested that the presence of small gold particles, as obtained by the SMAD technique, is not the main requisite for the achievement of the highest CO conversion. The strong interaction between ionic gold and ceria, by enhancing the ceria surface oxygen reducibility, may determine the particularly high activity.

Introduction

The interest in using gold as a catalyst component has increased during the last 15 years,[1] since the surprisingly high activity in CO oxidation at low temperature was reported for small (3−5 nm) gold particles supported on various oxides.[2,3] The catalytic applications of gold are indeed explored in several processes, such as NO removal,[4] catalytic combustion of volatile organic compounds VOC,[5,6] hydrotreatment,[7,8] chemical processing,[9−11] and also in the purification of hydrogen for fuel cell application.[12] However, the attainment of the best performing supported gold catalyst is still a challenge. The main reason for this is ascribed to the multiplicity of factors influencing the catalytic activity. The quantum size effect, observed in correspondence of the Au metal particle diameter of the order of 3.5 nm, was indicated as the main requisite for the high catalytic activity of the gold catalysts in the low-temperature oxidation of CO.[13,14] However, this effect, due to the particle size, could not explain alone the results obtained with different supports.[15] A distinction between "inert" and "active (or reducible)" oxides is generally made on the basis of their capability to adsorb oxygen.[16] With the "inert" class of oxides, characterized by a low ability to adsorb oxygen, the reaction proceeds through the dissociative adsorption of oxygen on the Au particles. The process is favored on a metal surface defect site (edge, kink, or step sites)[17,18] or on small particles with a changed electronic structure.[14,19] With the "active" class of oxides, oxygen is assumed to adsorb on the support where it may or may not dissociate before reacting with CO adsorbed on Au.[20,21] In this case, the activity behavior is sensitive to the microcrystalline structure of the metal−support interface, and therefore it depends on catalyst pretreatments.[16,22] Among the reducible oxides, CeO_2, characterized by a high oxygen storage capacity,[23] has lately been used as support for gold catalysts in a variety of reactions, such as the water−gas shift reaction,[5,24] the catalytic combustion of VOC,[6] and the low-temperature CO oxidation.[25,26] In all cases, gold improves the catalytic activity of ceria; however, no agreement has yet been found on the nature of the active sites. Some results indicate that metallic Au is the active site;[6] others highlight the role of the Au^+ and Au^{3+} species.[25,26]

To discriminate the activity of the different gold species on ceria, we prepared Au/CeO_2 catalysts by the classical deposition-precipitation method,[27,28] which is reported to form both metallic and ionic gold[6,29] and, by the solvated metal atom dispersion (SMAD) technique, producing in one step zerovalent gold atoms on the support without byproducts of the metal precursors.[30,31] For comparison, the coprecipitation method was also used. The samples, characterized by XRD, TPR, and XPS, were tested in the low-temperature oxidation of CO. The results of this investigation are here reported, and the catalytic performances are discussed in terms of the structural change of the support and of the electronic state of gold.

Experimental Section

Catalyst Preparation. Ceria-supported gold catalysts were prepared via two synthetic routes: deposition-precipitation (DP) and solvated-metal atom dispersion (SMAD). For the DP method, CeO_2 powder (from Aldrich, with a specific surface area = 79 $m^2\ g^{-1}$, pore size between 2 and 30 nm with a maximum at 2.4 nm, pH point of zero charge = 4.2) was suspended in distilled water under stirring. An appropriate volume of a 1.3×10^{-2} M water solution of $HAuCl_4$ was added to yield a final gold concentration of 5×10^{-4} M at a pH of around 6. After the suspension was stirred for 3 h at room temperature, Na_2CO_3 was added slowly until pH $\approx$ 8.5 was obtained. The solution was then kept refluxing and under stirring

* Corresponding author. Tel.: +39 0916809372. Fax: +39 0916809399. E-mail: anna@pa.ismn.cnr.it.
† Istituto per lo Studio dei Materiali Nanostrutturati.
‡ Università di Palermo.

10.1021/jp045928i CCC: $30.25
Published on Web 01/26/2005

overnight at 363 K. At the end of this step, the color changed from yellowish to beige. The precipitate was then filtered and washed with ammonia solution (pH = 8−9) until no chloride ions were detected by the $AgNO_3$ test. After a last rinsing in distilled water, the precipitate was dried at 393 K overnight. A gray solid was obtained.

The SMAD technique, according to ref 31, involved the following steps: (a) deposition of solvent (acetone) on the walls of the metal vapor reactor cooled at 77 K (liquid nitrogen temperature); (b) vaporization of the metal under vacuum followed by the rapid deposition of the atoms on the frozen solvent of the walls; and (c) warming up of the condensate of solvated gold atoms, and melting it down to the bottom of the reactor. The solution was then used to impregnate a weighted amount of ceria powder added into the reactor. The excess of solvent was removed in a vacuum at room temperature. A sample of light violet color was obtained.

For comparison, a catalyst with 10 wt % of gold was prepared by coprecipitation (CP). As will be explained later, the choice of this rather high gold loading and of this procedure aimed to reproduce a bulk composite compound, $Ce_{1-x}Au_xO_{2-\delta}$, with a gold concentration comparable to the one detected by XPS at the surface of the DP-prepared sample. According to the procedure, $HAuCl_4$ and $Ce(NO_3)_3 \cdot 6H_2O$ were mixed in aqueous solution with Na_2CO_3 at 298 K, keeping the pH at a constant value of 10 under stirring for 1 h.[32] The sample was then filtered and washed several times with hot water to eliminate all of the anions and the sodium arising from the precursors. The precipitate was dried at 393 K overnight and then calcined at 673 K for 4 h. Portions of the simply dried and of the calcined sample underwent structural analyses and catalytic tests.

The Au loading in the samples was determined by ICP-AES technique using the ICP Varian Vista MPX instrument. The catalysts prepared by DP and SMAD, containing 3 wt % of gold, are labeled as 3AuCe(DP) and 3AuCe(SMAD), respectively. The coprecipitated sample with 10 wt % of gold is indicated as 10AuCe(CP).

Catalyst Characterization. X-ray Diffraction. The X-ray diffraction measurements for the structure determination were carried out with a Philips (PW 1820) vertical goniometer using Ni-filtered Cu Kα radiation (λ = 1.5418 Å). A proportional counter and a 0.05° step size in 2θ were used. The assignment of the crystalline phases was based on the JPDS powder diffraction file cards.[33] The XRD data were analyzed according to the Rietveld method using the GSAS package program.[34,35] The particle sizes of different phases were calculated from the line broadening of the most intense reflections using the Scherrer equation.[36]

XPS Photoelectron Spectroscopy. The X-ray photoelectron spectroscopy analyses were performed with a VG Microtech ESCA 3000 Multilab, equipped with a dual Mg/Al anode. The spectra were excited by the nonmonochromatized Al Kα source (1486.6 eV) operated at 14 kV and 15 mA. The analyzer operated in the constant analyzer energy (CAE) mode. Survey spectra were measured at 50 eV pass energy. For the individual peak energy regions, a pass energy of 20 eV was used. The sample powders were pelletized and then mounted on a double-sided adhesive tape. The pressure in the analysis chamber was in the range of 10^{-8} Torr during data collection. The constant charging of the reference samples, pure ceria and pure gold, was corrected by referencing all of the energies to the C 1s peak energy set at 285.1 eV, arising from adventitious carbon. The binding energies of the catalysts were corrected with respect to the $Ce^{(IV)}$ $3d_{5/2}$ peak energy set at 882.0 eV, taken as internal reference peak. The peaks were fitted by a nonlinear least-squares fitting program using a properly weighted sum of Lorentzian and Gaussian component curves after background subtraction according to Shirley and Sherwood.[37,38] The relative atomic concentrations were calculated with the instrument-provided program, from fitted peak areas using appropriate sensitivity factors. The binding energy values are quoted with a precision of ±0.15 eV. The uncertainty on the atomic concentration is of the order of 10%.

H_2-TPR. Temperature programmed reduction (TPR) experiments were carried out with a Micromeritics Autochem 2910 apparatus equipped with a thermal conductivity detector (TCD). The reactor consisted of a quartz U-shaped tube where the sample (100 mg), diluted with inert SiC to avoid thermal gradients, was introduced. A thermocouple in contact with the catalytic bed allowed the control of the temperature inside the catalyst. Before the temperature programmed reduction was started, the samples were pretreated with a flowing gas mixture of 5% O_2 in He at atmospheric pressure, at 393 K for 1 h. The gas mixture of 5% H_2 in Ar was then left flowing on the samples with a flow rate of 30 mL/min, while heating from 253 to 1323 K at the rate of 10 K/min.

Catalytic Tests. Catalytic tests were performed in a pulse flow system using the same experimental setup of the TPR experiments. Before the catalytic tests, the samples were pretreated "in situ" under flowing 5% O_2 in He at 373 K for 0.5 h. A pretreatment at 623 K was needed for the SMAD sample to eliminate some residual organic solvent. For the catalytic CO oxidation, the reagent gas mixture consisting of 1% of CO + 1% of O_2 in He was led over 50 mg of catalyst at a total flow rate of 50 mL/min (STP), equivalent to a weight hourly space velocity (WHSV) of 60 000 mL g^{-1} h^{-1}. The CO and CO_2 effluent gases were monitored via an IR analyzer (ABB Uras 14). The conditions of kinetic regime were ascertained by varying the flow rates and the catalyst grams accordingly.

Results and Discussion

In Figure 1, the CO conversion as a function of the temperature from 173 to 723 K is displayed for pure ceria and for the differently prepared samples. In Table 1, the temperatures in correspondence of the 100% conversion are listed. As indicated by the lowering of this temperature, the addition of gold improves substantially the CO oxidation activity of the pure support; however, its effect is strongly dependent on the preparation method, with the largest activity exhibited by the DP sample, followed by the SMAD sample and with the CP sample showing the lowest activity. The DP sample just dried at 393 K was exceptionally active below room temperature with a specific rate of 6×10^{-6} mol CO s^{-1} g_{cat}^{-1} at 263 K. This value compares favorably with 2.2×10^{-6} mol CO s^{-1} g_{cat}^{-1} reported recently on Au/CeO_2[39] and with 3.5×10^{-6} mol CO s^{-1} g_{cat}^{-1} stated for Au/TiO_2 (3.3 wt %)[40] and appears to be the most active catalyst so far reported for this type of reaction. This catalyst exhibited a decrease of about 20−25% of the original activity, when tested after being 1 month old (naturally aged inside a close vial). A 10% deactivation was observed after 40 h of time on stream at room temperature. A portion of the 10AuCe(CP), just dried at 393 K, tested in the same reaction, displayed a lower CO conversion as compared to the 673 K calcined sample.

In Table 2, the support crystallite sizes and the average gold particle sizes as determined from the line broadening of the metal Au (111) XRD peak are listed. No gold particles are detected by the XRD measurements on the DP and the CP

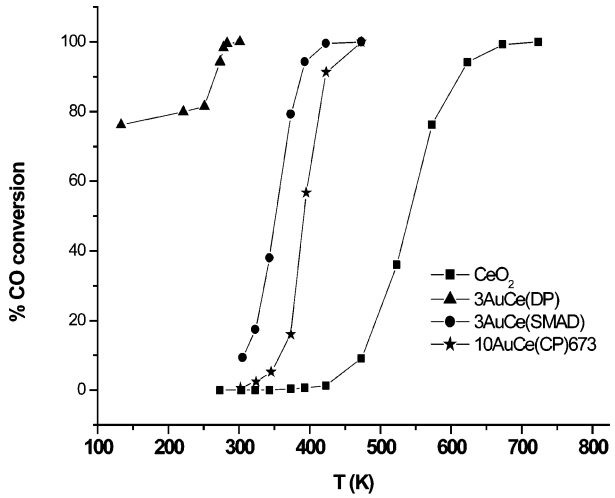

Figure 1. CO conversion % as a function of temperature for the different catalysts.

TABLE 1: Temperature in Correspondence of the 100% Conversion of CO

catalyst	$T_{100\%}$ (K)
$3AuCe(DP)_{393K}$	301
$3AuCe(DP)_{1monthaged}$	373
$3AuCe(SMAD)_{298K}$	427
$10AuCe(CP)_{673K}$	473
ceria	723

TABLE 2: Average Ceria Crystallite Size, d_{CeO2}, and Au Particle Size, d_{Au}, As Obtained from XRD Analyses of the Different Catalysts (Values Are Quoted with an Uncertainty of ±10%)

catalyst	d_{CeO2}[a] (nm)	d_{Au} (nm)
$3AuCe(DP)_{393K}$	22, 8	n.d.
$3AuCe(SMAD)_{298K}$	22, 8	n.d.
$3AuCe(SMAD)_{623K}$	22	2.5
$3AuCe(SMAD)_{773K}$	22	5.0
$10AuCe(CP)_{393K}$	n.d.	n.d
$10AuCe(CP)_{673K}$	10	8.0

[a] The first value refers to the pure ceria, and the second one refers to the composite gold−ceria phase.

samples simply dried at 393 K and on the SMAD sample just after vacuum-drying it at room temperature. Gold particles of XRD detectable size, increasing with the calcination temperature, are obtained on the SMAD and CP samples after calcination at higher temperature. Addition of gold to ceria by DP and by SMAD techniques did not change the surface area with respect to the pure ceria value of 79 m^2/g. The coprecipitation sample exhibits a lower BET area of 40 m^2/g.

The XRD patterns of the SMAD sample "as prepared", after oxygen treatment at 623 K and after oxygen treatment at 773 K, are shown in Figure 2. As indicated by the narrowing of the Au (111) reflection peak, shown in the inset of the figure, sintering of the gold particles with the increasing temperature occurred. The corresponding particle sizes are reported in Table 2. In correspondence of a size increase from 2.5 to 5 nm, only a slight decrease in activity was observed, suggesting that in this case particle size effects were not relevant.[5,6] The observed and calculated XRD patterns of the DP sample and pure support are given in Figure 3. As shown in the inset, differences between the two sample patterns become more evident at high 2θ. The experimental data were fitted by two curves, slightly shifted, one with respect to the other. The two curves are indicative of two different phases: one due to pure ceria, characterized by the fluorite structure with a calculated lattice parameter of 5.416 Å, and the other phase still of fluorite structure with a contracted lattice parameter of 5.403 Å, attributed to a solid solution between gold and ceria. The closeness of the ionic radii of Ce^{4+} and Au^{3+}, 0.97 and 0.85 Å, respectively,[41] would indeed allow for the formation of a composite $Ce_{1-x}Au_xO_{2-\delta}$ (where δ takes into account the charge balance).[25,26] The XRD pattern of the CP sample calcined at 673 K is shown in Figure 4. Differently from the DP sample, and as expected from the high-temperature treatment, this profile reveals the Au (111) and the Au (200) reflection peaks of metallic gold along with the peaks related to the CeO_2 phase with a certain degree of amorphism. It is worth mentioning that the further calcinations of the CP sample at 673 K aimed to form the solid solution, with a modified fluorite structure of ceria, which appeared to be amorphous after the 393 K treatment. Moreover, for the purpose of this study, the attainment of just ionic gold species by the DP method followed by the mild treatment in air at 393 K fulfilled our original objective.

In Table 3, the results in terms of the main binding energies, Au $4f_{7/2}$, O 1s, of Au/Ce atomic ratio and gold loading, as obtained from the XPS quantitative analyses, are reported for the differently prepared samples. For all samples, no extra peaks due to impurities were observed. In consideration of the decreased activity of the 3AuCe(DP) with aging and after the catalytic reaction, the XPS results of this sample at different stages of its life, referred to as "as prepared", "aged", and "used", are listed in the table. Because no such changes in activity were observed with the samples prepared by the other two techniques, no distinction between different stages of the catalyst life is done and only the XPS data of the fresh samples are reported. The energy differences between the $Ce^{(IV)}$ $3d_{5/2}$ and the main energy component of Au $4f_{7/2}$ are also included in the table. Indeed, this difference being independent from energy reference effects, its value is a reliable indication of the real change in the gold binding energies (of course assuming that the ceria binding energy is not modified by the presence of gold and that differential charging effects are negligible). The experimental and the fitted spectra of the Au 4f region of 3AuCe(SMAD) and 3AuCe(DP) are shown in Figure 5. The Au 4f ionization process is characterized by the doublet of the two spin−orbit components, Au $4f_{7/2}$ and Au $4f_{5/2}$, with a splitting of 3.7 eV. As indicated in the figure, the experimental curves were fitted with two doublets. The SMAD prepared sample presents a main Au $4f_{7/2}$ component at a binding energy of 84.1 eV typical of metallic gold,[25] and a quite small component at 86.1 eV, likely due to oxidized surface gold species. It is worth noticing that the Au 4f spectral features of the SMAD sample just dried and after being calcined did not change. The 3AuCe(DP) sample analyzed just as soon as prepared is characterized by two Au 4f components, one with the Au $4f_{7/2}$ at 85.6 eV and the other with Au $4f_{7/2}$ at 87.5 eV. In consideration of the fact that all of the chlorine was eliminated by the washing procedure, as was also proved by the absence of any chlorine peak in the corresponding photoelectron energy region, the two gold components observed in the DP prepared sample must be attributed to Au−oxygen-containing species of the Au^+ and Au^{3+} types. According to the quantitative XPS analyses, the DP method afforded a much better dispersion of the gold on the surface of the support. The modification of the Au 4f signal of the 3AuCe(DP) with the aging time and upon the long time stability test is shown in Figure 6. The corresponding XPS data are also included in Table 3. The aged sample is characterized by the two Au $4f_{7/2}$ components

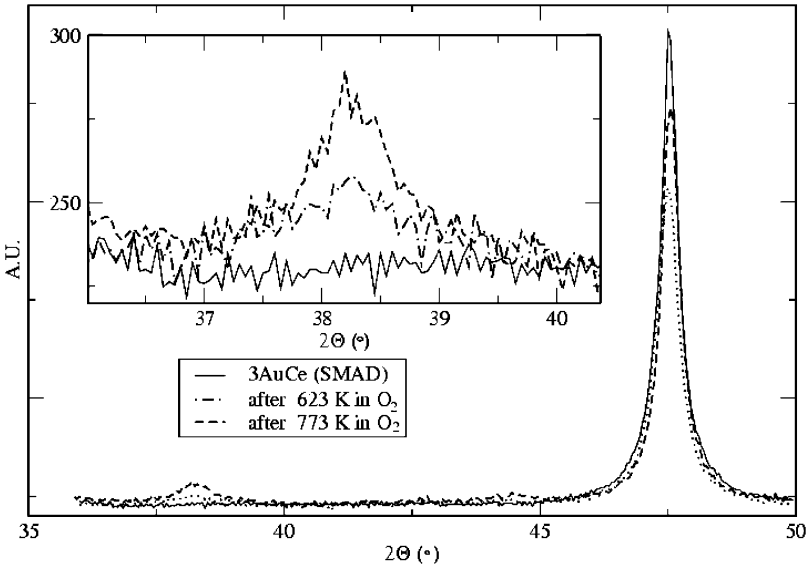

Figure 2. XRD patterns of the 3AuCe(SMAD) after different treatments. The enlargement of the Au (111) peak is shown in the inset.

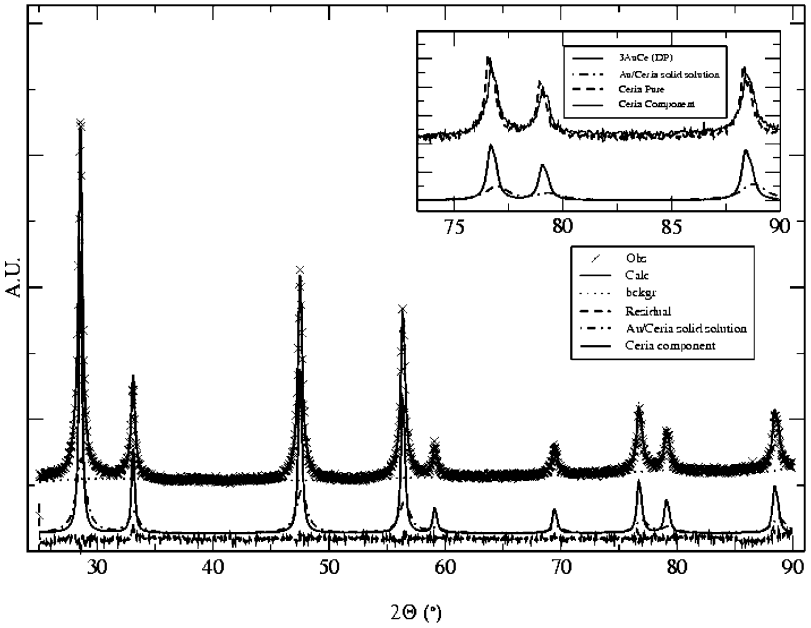

Figure 3. Observed and calculated XRD pattern of 3AuCe(DP) sample along with the pure ceria pattern. The enlargement of the high angle region is shown in the inset.

downshifted to 85.1 and 87.2 eV, respectively, and by a decrease of the surface gold species with respect to cerium. The overall negative shift of the gold binding energies could be interpreted as a spontaneous tendency of the gold to reduce its oxidation states by segregating out of the ceria lattice. Therefore, the lack of this "aging" effect in the SMAD and in the CP (calcined at 673 K) samples could be attributed to the metallic nature of gold already present in the "as prepared" states. The lowering of the Au/Ce atomic ratio is in accord with an agglomeration of the gold-containing phase. These electronic and morphological changes detected by XPS may then be responsible for the observed deactivation of the catalyst with aging time. After the catalytic test, the Au $4f_{7/2}$ and Au $4f_{5/2}$ components are better resolved, due to the almost unique presence of the Au^+ species. No further shift of the Au 4f binding energies is observed upon reaction; however, the decrease of the Au^{3+} component could be a consequence of the reducing action of the CO.[42] To follow the electronic and morphological changes that occurred during the steps of the coprecipitation procedure, the X-ray photoelectron spectra of the CP sample after the drying process at 393 K and after calcination at 673 K were collected and shown in Figure 7. The coprecipitation sample dried at 393 K is characterized by a very small surface gold concentration and by two Au 4f doublets with Au 4 $f_{7/2}$ components at 85.4 and 87.8 eV, respectively, attributed to Au^+ and Au^{3+}. After calcination at 673 K, both components are shifted, respectively, to 84.5 eV, quite close to the binding energy of Au°, and to 86.1 eV typical of charged gold. Moreover, upon the high temperature calcination, the surface Au/Ce atomic ratio increases noticeably. Such an increase indicates, in accord with XRD results, a temperature-driven outward diffusion of gold as metallic particles. The XPS results for the calcined CP sample are qualitatively very similar to those obtained for the SMAD sample. However, the quantitative analysis yields a much lower surface gold concentration as compared to the 3AuCe(SMAD) sample. The lower amount of XPS-detected gold reflects the major disadvantage associated with the coprecipitation method consisting of the burial of the active species within the support.[1]

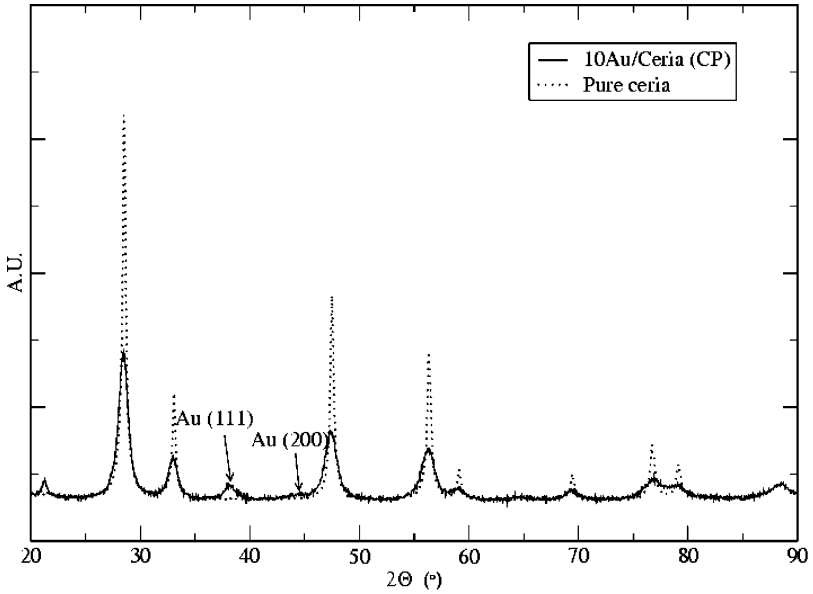

Figure 4. Observed XRD pattern of the 10AuCe(CP) and pure ceria support.

TABLE 3: Au $4f_{7/2}$, O 1s Binding Energies, Au/Ce Atomic Ratios, [$Ce^{(IV)}$ $3d_{5/2}$ − Au $4f_{7/2}$], and XPS wt % Au of the Various Gold Samples (fwhm (eV) in Parentheses and Percentages of the Chemical Species Are Also Given)

sample	Au $4f_{7/2}$ (eV)	O 1s (eV)	Au/Ce	[Ce $3d_{5/2}$ − Au $4f_{7/2}$] (eV)	Au (wt %)
3.0AuCe(DP)	85.6 (2.2) 79%	529.9 (1.9) 70%	0.071	796.2	8
(as prepared)	87.5 (2.2) 21%	531.5 (1.9) 23%			
		533.3 (1.9) 7%			
3.0AuCe(DP)	85.1 (2.1) 77%	529.5 (1.9) 74%	0.049	796.9	5.6
(aged)	87.3 (2.1) 23%	531.4 (1.9) 20%			
		533.2 (1.9) 6%			
3.0AuCe(DP)[a]	85.1 (2.1) 94%	529.6 (2.1) 66%	0.040	796.9	4.6
(used)	87.2 (2.1) 6%	532.2 (2.1) 34%			
10AuCe(CP)	85.4 (2.1) 81%	529.7 (2.2) 34%	0.003	796.6	0.3
calc. 393 K	87.8 (2.1) 19%	531.5 (2.2) 58%			
		533.2 (2.2) 8%			
10AuCe(CP)	84.5 (2.0) 72%	529.6 (2.4) 73%	0.011	797.2	1.3
calc. 673 K	85.8 (2.0) 28%	531.7 (2.4) 22%			
		533.8 (2.4) 5%			
3AuCe(SMAD)	84.1 (1.9) 93%	529.6 (2.3) 73%	0.036	797.9	4
	86.1 (1.9) 7%	532.0 (2.3) 21%			
		533.8 (2.3) 6%			

[a] After 40 h of time on stream at room temperature.

The Ce 3d spectra of the dried and calcined 10AuCe(CP) are shown in Figure 8a and b, respectively. The experimental curves were fitted with several components arising from the multiplicity of final states reached during the Ce 3d photoionization process.[43] The oxidation of the Ce(III) after calcinations at 673 K is clearly indicated by the decrease of the V′ peak, attributed to the Ce $3d_{5/2}$ component of a Ce(III). The spectrum of Figure 8b, related to the calcined sample, is typical of the pure CeO_2 spectrum, and it is representative of the other samples. It is worth saying that the pure ceria contains always a small percentage (about 6%) of Ce(III) oxide and that some reduction is induced by the X-ray exposure. In all of the analyzed samples, the O 1s spectra (not shown) consisted mainly of two peaks, a dominant one at energy ∼529 eV due to the lattice oxygen from the CeO_2 and the other at a higher binding energy around 531 eV due to hydroxide species.[44] The presence of Ce^{3+}-related surface defects leads to a weak component at an even higher energy of ∼533.5 ± 0.5 eV.[43]

To investigate the reactivity changes of the ceria support upon gold addition, the H_2 temperature programmed reduction was performed on the differently prepared samples. The TPR patterns of the analysed samples and of the pure ceria support are shown in Figure 9. The temperatures of the peak maxima are given in Table 4. As reported in the literature, ceria is characterized by a low-temperature peak at 684 K, attributed to the reduction of the surface oxygen species, and a high-temperature peak at 1080 K, due to bulk oxygen species.[5,6] According to literature, the high-temperature peak of the gold/ceria catalysts remains unchanged, whereas the low-temperature peak shifts to low temperature[29] as an indication of the increased surface oxygen reducibility. The most important differences among the analyzed samples lie in the extent of this temperature shift. The DP sample exhibits a shift of about 340 K, the SMAD of about 300 K, and the CP sample of 245 K. Moreover, in the TPR profile of the SMAD sample, a small peak in correspondence of the low-temperature peak of the pure support is observed. The presence of such peak may be indicative of a nonuniform distribution of gold particles, leaving unaffected a part of the ceria surface. In agreement with previous studies, for the DP sample, the peak at low temperature should contain a contribution from the reduction of the surface ceria and from the reduction of the ionic gold species.[24] This last contribution, estimated to be of the order of 2−3 mL/g, is slightly above the experimental error, as reported in Table 4, but it was confirmed by the negative

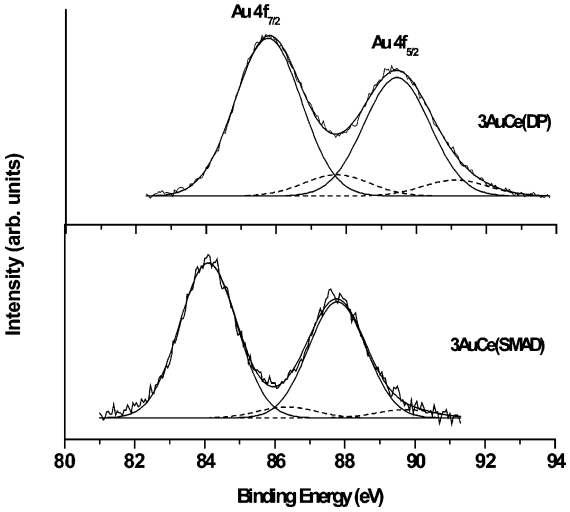

Figure 5. Experimental and fitted Au 4f photoelectron peaks of the samples prepared by deposition-precipitation and by SMAD technique. The solid and dashed lines indicate two different doublet components.

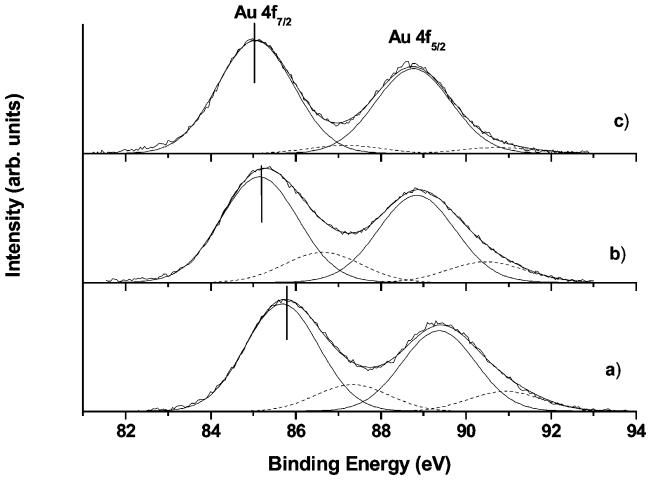

Figure 6. Experimental and fitted Au 4f peaks of the 3AuCe(DP): (a) as prepared, (b) after 1 month, and (c) after 40 h on stream.

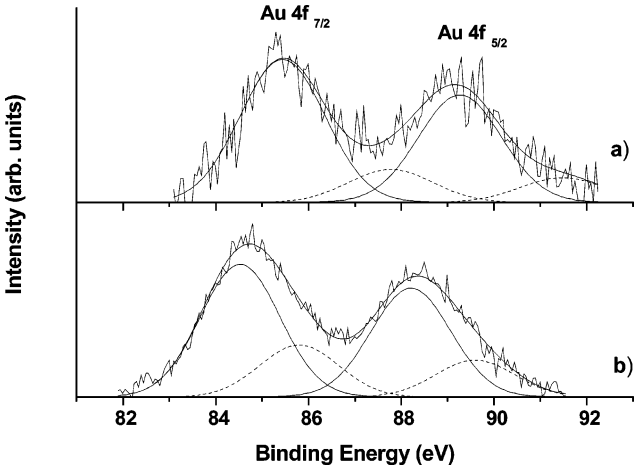

Figure 7. Experimental and fitted Au 4f XP spectra of 10AuCe(CP), calcined (a) at 393 K and (b) at 673 K. The solid and dashed lines indicate two different doublet components.

chemical shift of the Au $4f_{7/2}$ found for the sample analyzed after stopping the TPR at 473 K and indicative of reduced gold. The larger consumption of hydrogen, observed in the surface and bulk peaks of the CP sample, may be due to the presence of smaller ceria crystallites sizes[23] (see Table 1). The increased

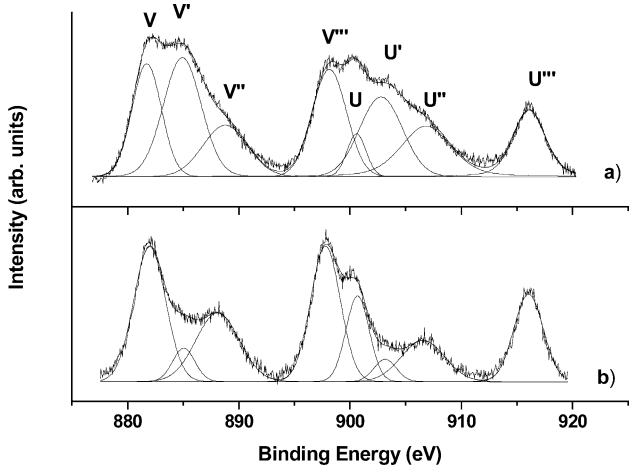

Figure 8. Experimental and fitted Ce 3d XP spectra of 10AuCe(CP) calcined at (a) 393 K and (b) 673 K.

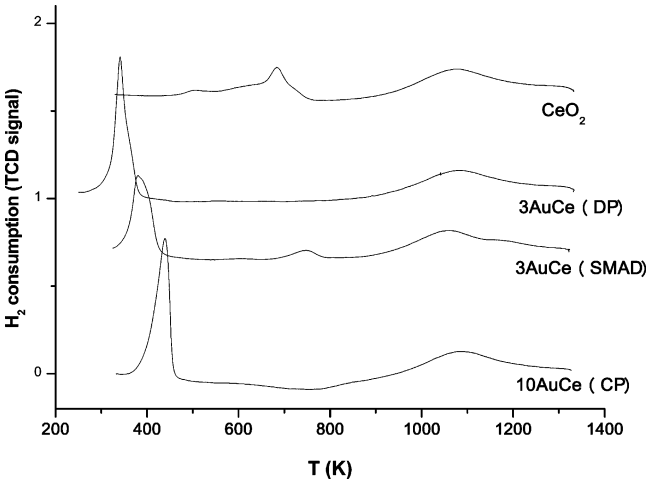

Figure 9. H_2-TPR pattern of the various samples.

TABLE 4: TPR Peak Maxima (±15 K) and H_2 Uptake (±15%) of Pure Ceria and of Au/CeO_2 Samples

sample	T_1 (K)	V_1 (mL/g)	T_2 (K)	V_2 (mL/g)
CeO_2	1080	17	684	9
3AuCe(DP)	1082	19	341	11
3Auce(SMAD)	1059	16	380	8
10AuCe(CP)	1082	23	439	10

reducibility of the surface oxygen of ceria, associated with the low-temperature peak shift, may imply different mechanisms depending on whether it is induced by gold metal or gold ions. In analogy with other noble metals, and as shown for gold supported on different oxides, metallic gold could indeed activate the hydrogen with subsequent spillover on the support and promotion of the ceria reduction at lower temperature.[45] In this case, the process would be favored by a high dispersion of gold on the surface.[1] We may invoke such a mechanism for the SMAD and CP_{673K} samples and therefore explain the higher reducibility of the SMAD sample by the presence of smaller gold particles with respect to the CP sample. In the case of the deposition-precipitation sample, containing only ionic gold, as ascertained by XRD and XPS, the surface oxygen reducibility may be enhanced through a lattice substitution mechanism.[29] Accordingly, the ions Au^+ or Au^{3+} would fill the vacant Ce^{4+} sites with consequent formation of oxygen vacancies and increased oxygen mobility and reducibility. The more effectiveness of this mechanism as compared to the metallic hydrogen spillover is indicated by the large shift of the surface oxygen

reduction peak observed for the 3AuCe(DP) (Table 3). Indeed, diffusion of gold ions is thermodynamically a more favored process as compared to the hydrogen activation by metallic gold.[18]

From the linear relationship observed between the reducibility of the surface ceria oxygen and the catalytic activity, it may be inferred that the CO oxidation is affected by the same factors influencing the TPR process. The presence of the metallic gold in the SMAD and the CP catalysts, in analogy with other noble metals, will weaken the C−O bond and therefore make easy the further insertion of oxygen with release of CO_2.[46] In the case of the DP sample containing ionic gold species, the increased activity for the CO oxidation could be attributed to the weakening of the Ce−O bond and the increased oxygen mobility. In this case, the ionic species in intimate contact with the ceria lattice would act as a modifier of the ceria properties.[29]

From this study, the following results can be summarized: (i) it is possible to design a gold on ceria catalyst with well-defined gold chemical species; (ii) the SMAD method produces gold particles of very small sizes, while the deposition-precipitation method with a mild drying at 393 K produces only ionic gold in such an intimate contact with the ceria to form a fluorite type structure of a mixed phase $Au_xCe_{1-x}O_{2-\delta}$ with a contracted lattice; and (iii) the failed attempt to prepare a composite Au−ceria massive compound by coprecipitation showed that, to insert gold into the ceria lattice, we must have an already preformed ceria phase in which the diffusion of gold ions through the lattice or through the grain boundaries prevails over its tendency to agglomerate and form metallic particles. Indeed, the calcination at 673 K has produced mainly metallic gold particles still buried inside the ceria matrix. The last but not the least important result is that the deposition-precipitation method without high temperature calcinations allows one to obtain an extraordinarily active Au/ceria catalyst for the low-temperature oxidation of CO.

The detailed investigation of the effect of calcination temperature, metal loading, and support crystallinity on the activity of a DP catalyst will be described in a forthcoming paper.

Conclusion

According to the structural and surface characterization, the three adopted syntheses for the ceria-supported gold catalysts have produced materials with different structural, morphological, and electronic properties. The sample prepared by deposition-precipitation, despite the mild treatment at 393 K, was characterized by the presence of a mixed oxide $Au_xCe_{1-x}O_{2-\delta}$ and, according to XPS, contained only ionic gold. On the contrary, the SMAD and the CP samples, treated at high calcination temperatures, contain the pure fluorite phase of the support and metallic gold. The catalytic activity of the DP sample at 263 K was exceptionally high (specific rate $= 6 \times 10^{-6}$ mol of CO s^{-1} g of cat^{-1}) and quite stable during reaction. The linear relationship between the activity of the catalysts, and the oxygen surface reducibility as obtained by the H_2-TPR, suggests that the same factors affecting the reducibility of the ceria are likely to affect the oxidation of CO. The presence of ionic gold in intimate contact with ceria, as in the DP case, contributes to the Ce−O weakening, differently from the case of metallic gold dispersed on the support surface.

Acknowledgment. Support by the European Community, Grant COST, Project D 15, is acknowledged.

References and Notes

(1) Bond, G. C.; Thompson, D. T. *Catal. Rev.-Sci. Eng.* **1999**, *41*, 319.
(2) Haruta, M.; Tsubota, S.; Kobayashi, T.; Kageyama, H.; Genet, M. J.; Delmon, B. *J. Catal.* **1993**, *144*, 175.
(3) Haruta, M.; Yamada, N.; Kobayashi, T.; Iijima, S. *J. Catal.* **1989**, *115*, 301.
(4) Ueda, A.; Haruta, M. *Gold Bull.* **1999**, *32*, 32.
(5) Fu, Q.; Weber, A.; Flytzani-Stephanopoulos, M. *Catal. Lett.* **2001**, *77*, 87.
(6) Scirè, S.; Minicò, S.; Crisafulli, C.; Satriano, C.; Pistone, A. *Appl. Catal., B* **2003**, *40*, 43.
(7) Venezia, A. M.; La Parola, V.; Nicolì V.; Deganello, G. *J. Catal.* **2002**, *212*, 56.
(8) Venezia, A. M.; La Parola, V.; Deganello, G.; Pawlec, B.; Fierro, J. L. G. *J. Catal.* **2003**, *215*, 317.
(9) Hutchings, G. J. *Catal. Today* **2002**, *72*, 11.
(10) Mohr, C.; Hfmeister H.; Claus, P. *J. Catal.* **2003**, *213*, 86.
(11) Nkosi, B.; Adams, M. D.; Covile, N. J.; Hutchings, G. J. *J. Catal.* **1991**, *128*, 378.
(12) Cameron, D.; Holliday, R.; Thompson, D. *J. Power Sources* **2003**, *118*, 298.
(13) Haruta, M. *Catal. Today* **1997**, *36*, 15.
(14) Valden, M.; Lai, X.; Goodman, D. W. *Science* **1998**, *281*, 1647.
(15) Grisel, R.; Westrate, K.-J.; Gluhoi, A.; Nieuwenhuys, B. *Gold Bull.* **2002**, *35*, 39.
(16) Schubert, M. M.; Hackenberg, S.; van Veen, A. C.; Muhler, M.; Plzak, V.; Behm, R. J. *J. Catal.* **2001**, *197*, 113.
(17) Hammer, B.; Norskov, J. K. *Nature* **1995**, *376*, 238.
(18) Xu, Y.; Mavrikakis, M. *J. Phys. Chem. B* **2003**, *107*, 9298.
(19) Guczi, L.; Petö, G.; Beck, A.; Frey, K.; Geszti, O.; Molnar, G.; Daróczi, C. *J. Am. Chem. Soc.* **2003**, *125*, 4332.
(20) Liu, H.; Kozlov, A. I.; Kozlova, A. P.; Shido, T.; Asakura, K.; Iwasawa, Y. *J. Catal.* **1999**, *185*, 252.
(21) Frost, J. C. *Nature* **1988**, *18*, 577.
(22) Kang, Y.-M.; Wan, B.-Z. *Catal. Today* **1995**, *26*, 59.
(23) Trovarelli, A. *Catal. Rev.-Sci. Eng.* **1996**, *38*, 439.
(24) Andreeva, D.; Idakiev, V.; Tabakova, T.; Ilieva, L.; Falaras, P.; Bourlinos, A.; Travlos, A. *Catal. Today* **2002**, *72*, 51.
(25) Bera, P.; Hegde, M. S. *Catal. Lett.* **2002**, *79*, 75.
(26) Liu, W.; Flytzani-Stephanopoulos, M. *J. Catal.* **1995**, *153*, 317.
(27) Tsubota, S.; Haruta, M.; Kobayashi, T.; Ueda, A.; Nakahara, Y. In *Preparation of Catalysts V*; Poncelet, G., et al., Eds.; Elsevier Science B. V.: New York, 1991; pp 695−704.
(28) Wolf, A.; Schüth, F. *Appl. Catal., A* **2002**, *226*, 1.
(29) Fu, Qi; Saltsburg, H.; Flytzani-Stephanopoulos, M. *Science* **2003**, *301*, 935.
(30) Klabunde, K. *Acc. Chem. Res.* **1975**, *8*, 399.
(31) Stoeva, S. I.; Prasad, B. L. V.; Uma, S.; Stoimenov, P. K.; Zaikovski, V.; Sorensen, C. M.; Klabunde, K. A. J. *J. Phys. Chem. B* **2003**, *107*, 7441.
(32) Luengnaruemitchai, A.; Osuwan, S.; Gulari, E. *Int. J. Hydrogen Energy* **2004**, *29*, 429.
(33) JCPDS Powder Diffraction File, Int. Centre for Diffraction Data, Swarthmore.
(34) Rietveld, H. M. *J. Appl. Crystallogr.* **1969**, *2*, 357.
(35) Young, R. A.; Prince, E. *J. Appl. Crystallogr.* **1982**, *15*, 357.
(36) Klug, H. P.; Alexander, L. E. *X-ray Diffraction Procedures for Polycrystalline and Amorphous Materials*; Wiley: New York, 1954.
(37) Shirley, D. A. *Phys. Rev. B* **1972**, *5*, 4709.
(38) Sherwood, P. M. A. In *Practical Surface Analysis*; Briggs, D., Seah, M. P., Eds.; Wiley: New York, 1990; p 181.
(39) Carrettin, S.; Concepcìon, P.; Corma, A.; Lopez Nieto, J. M.; Puntes, V. F. *Angew. Chem., Int. Ed.* **2004**, *43*, 2538.
(40) Tsubota, S.; Nakamura, T.; Tanaha, K.; Haruta, M. *Catal. Lett.* **1998**, *56*, 131
(41) Shannon, R. D. *Acta Crystallogr., Sect. A* **1976**, *32*, 751.
(42) Guzman, J.; Gates, B. C. *J. Am. Chem. Soc.* **2004**, *126*, 2672.
(43) Pfau, A.; Schierbaum, K. D. *Surf. Sci.* **1994**, *321*, 71.
(44) Paparazzo, E.; Ingo, G. M.; Zacchetti, N. *J. Vac. Sci. Technol., A* **1991**, *9*, 1416.
(45) Boccuzzi, F.; Chiorino, A.; Manzoli, M.; Tabakova, T. *J. Catal.* **1999**, *188*, 176.
(46) Serre, C.; Garin, F.; Belot, G.; Maire, G. *J. Catal.* **1993**, *141*, 1.